J Mater Sci (2009) 44:1613–1621
DOI 10.1007/s10853-008-3231-8

Effect of highly dispersible zirconia nanoparticles on the properties of UV-curable poly(urethane-acrylate) coatings

Kun Xu · Shuxue Zhou · Limin Wu

Received: 17 August 2008 / Accepted: 29 December 2008 / Published online: 27 January 2009

Abstract Highly crystalline and dispersible zirconia nanoparticles, ex situ synthesized from a solvothermal reaction of zirconium(IV) isopropoxide isopropanol complex in benzyl alcohol, were functionalized with 3-(trimethoxysilyl)propyl methacrylate and blended with UV-curable urethane-acrylate formulations to fabricate poly(urethane-acrylate)/zirconia (PUA/ZrO_2) nanocomposite coatings. A critical ZrO_2 concentration of 20 wt% was observed for the evolutions of both the structure and properties of the nanocomposites as a function of ZrO_2 content. Below the critical concentration, completely transparent nanocomposite film was obtained and the nanocomposites exhibited increasing final carbon–carbon double bond conversion, refractive index, hardness, elastic modulus, and thermal stability as ZrO_2 content increased. However, serious agglomeration of ZrO_2 nanoparticles occurred at 25 wt% of ZrO_2, which decreased final conversion, transparency and hardness, and thermal stability of the nanocomposite film. These results clearly reveal that the performance of UV-curable nanocomposites is strongly dependent on the dispersion of nanoparticles.

Introduction

Polymer-based nanocomposites have drawn considerable attention in recent years because of their prominent mechanical, optical, electrical, thermal properties, and so on [1–3]. These nanocomposites can be fabricated by blending or a sol–gel process, especially, the blending method would be preferred due to its simple and feasible industrialization. However, how to prepare transparent nanocomposite particularly with high nanofiller load using blending technique still remains a great challenge, which lies in the difficult de-aggregation of commercial nanopowder and inherently poor miscibility between polymer and inorganic nanoparticles.

Up to now, various types of oxide nanoparticles such as silica [4–6], titania [7], alumina [8], zinc oxide [9], and ITO [10], have been introduced into polymer matrix by multifarious blending processes to understand their influences on the hardness, strength, abrasion resistance, scratch resistance, and weatherability of the polymer or to endow them with new functionalities, i.e., UV-blocking, antibacterial, and electric conductive properties. But zirconia nanoparticles are seldom involved. Zhou et al. [11] ever employed zirconia nanopowder to reduce the thermal expansion coefficient of poly(ether-sulfone) for meeting its application in the connector of optical fiber. Recently, Lee et al. [12] prepared transparent ZrO_2–polydimethylsiloxane (PDMS) nanocomposites by dispersing ZrO_2 nanoparticles in a PDMS matrix via ligand molecule engineering. A high refractive index of 1.65 was reached at 20.8 vol.% of ZrO_2 content. However, the other properties of the nanocomposites were not concerned.

In this article, a kind of highly crystalline ZrO_2 nanoparticles, synthesized from a solvothermal reaction of zirconium(IV) isopropoxide isopropanol complex in benzyl alcohol [13], is employed to fabricate nanocomposite coatings with high performances. These nonaqueous synthesized ZrO_2 nanoparticles are highly dispersible in organic media with the aid of ligands, as described in our

K. Xu · S. Zhou (✉) · L. Wu
Department of Materials Science and Advanced Coatings Research Center of China Educational Ministry, Fudan University, Shanghai 200433, People's Republic of China
e-mail: zhoushuxue@fudan.edu.cn

previous publication [14], and have been successfully utilized to fabricate photopolymerized nanocomposites for volume holographic gratings with the highest refractive index contrast (n1 of up to 0.024) [13] as well as for scratch resistant coatings for polycarbonate [15]. However, completely transparent nanocomposite coatings were achieved only below 10 wt% of ZrO_2 when the ZrO_2 nanoparticles were functionalized with 3-(trimethoxysilyl)propyl methacrylate (MPS) and blended with pure polyurethane (PU) oligomer. Herein, the PU oligomer was replaced by a composition composing of PU oligomer, isobornyl acrylate, and 1,6-hexanediol diacrylate (HDDA), based on a weight ratio of 52.5:17.5:30. Completely transparent UV-cured poly(urethane-acrylate) (PUA)/ZrO_2 nanocomposite films with as high as 20 wt% of ZrO_2 were obtained. The final carbon–carbon double bond conversion, the optical and mechanical properties as well as the thermal stability of the nanocomposites as a function of ZrO_2 load were comprehensively investigated.

Experimental

Materials

Zirconium isopropoxide isopropanol complex (99.9%) and anhydrous benzyl alcohol (99%) were purchased from Aldrich and MPS from Sigma. Aliphatic urethane diacrylate (6148J-75, composing of 75 wt% of PU oligomer and 25 wt% of isobornyl acrylate) was kindly offered by Eternal Chemical Corp., Ltd. (China). HDDA and 1-hydroxy-cyclohexyl-phenyl-ketone (Iragure 184) were got from Shanghai Baorun Chemical Corp., Ltd. (China). Tetrahydrofuran (THF, ≥99.5%), absolute ethanol (>99.7), and methanol (≥99.9%) were obtained from Sinopharm Chemical Reagent Corp. All chemicals were used as received.

Synthesis of highly crystalline zirconia nanoparticles

ZrO_2 nanocrystals were synthesized according to the procedure described elsewhere [13, 14, 16]. That is, 3.33 g of zirconium(IV) isopropoxide isopropanol complex and 50 mL of benzyl alcohol were charged into a 100-mL Teflon liner. Subsequently, the Teflon liner was slide into a stainless steel autoclave and carefully sealed. The autoclave was put into an oven at a temperature of 240 °C to carry out the reaction. After 4 days, the reaction mixture was allowed to cool down, and a white turbid suspension was obtained. The product was cubic ZrO_2 nanocrystal with monodisperse particle size of 3.8 nm and 9.2 g/100 g ZrO_2 of organic component was inherently chemically adsorbed on the as-synthesized ZrO_2 nanoparticles [17].

Preparation of MPS-functionalized zirconia nanoparticles dispersions

The as-synthesized ZrO_2 nanoparticles suspension in benzyl alcohol (solid content: 33 mg/g) was centrifuged to remove the benzyl alcohol and then washed with absolute ethanol three times. MPS and THF were then mixed with the wet ZrO_2 nanoparticles according to the molar ratios of MPS to as-synthesized ZrO_2 (0.05–0.20:1) and 1.2 wt% of ZrO_2. The mixture was sonicated at room temperature for 30 min and then heated at 60 °C for 24 h, followed by centrifugation at 8000 rpm for 10 min to remove the possible ZrO_2 aggregates. The obtained transparent ZrO_2/THF dispersions were concentrated to about 10 wt% of solid content using a rotary evaporator. Obviously, these dispersions contained a certain amount of free MPS molecules. A MPS-functionalized ZrO_2 nanoparticles dispersion without free MPS molecules was further fabricated for the case at 0.20:1 of MPS-to-ZrO_2 molar ratio. Namely, the corresponding free MPS-containing ZrO_2 dispersion was poured with fivefold volume of methanol, and then centrifuged to get the MPS-functionalized ZrO_2 nanoparticles. These MPS-functionalized ZrO_2 nanoparticles were further washed with methanol for two times to remove free MPS molecules. Thermogravimetric analysis indicated the MPS-functionalized ZrO_2 nanoparticles had 9% of weight loss more than the as-synthesized ZrO_2 nanoparticles in the range of 170–750 °C, meaning that the number of C=C double bond attached to each ZrO_2 nanoparticle (size: 3.8 nm) is 29.2–34.0 (assuming that MPS was bonded in terms of T^2 and T^3 structure). The wet MPS-functionalized ZrO_2 nanoparticles were dispersed in THF again to form a MPS-functionalized ZrO_2/THF dispersion with 15 wt% of ZrO_2 concentration.

Preparation of PUA/ZrO_2 nanocomposite coatings

Aliphatic urethane diacrylate (6148J-75) and HDDA were mixed first based on the weight ratio of 7:3 to compromise the toughness and hardness, which was acted as pure PUA mixture in this work. The PUA mixture was further blended with a certain amount of MPS-functionalized ZrO_2/THF dispersion by stirring, and evaporated under vacuum at 50 °C for 5 h to remove all THF. Afterward, 5 wt% of Iragure 184 (based on the weight of pure PUA mixture) was added to get a UV-curable coating. The coating was spin-coated on silicon wafer at a spinning speed of 3000 rpm for 1 min or cast on glass slides using a wire-wounded applicator, and then exposed to a UV lamp (power: 2 kW, maximal peak: 365 nm) for curing. The average thickness of the UV-cured coating on glass substrate was determined by a thickness gauge (Shanghai No. 4 Chemical Mechanics Factory, China).

Characterization

The photopolymerization kinetics was determined by real-time Fourier transformed infrared (FTIR) spectrometer (Nicolet 5700, Thermo Electron, USA). The liquid formulation was cast onto a silicon wafer and then exposed to a visible spot light source (10 mw/cm^2, EFOS Lite, Canada) at room temperature. A horizontal transmission accessory was designed to enable mounting of the sample in a horizontal orientation. The carbon–carbon double bond conversion was determined from the change of the peak at 6160 cm^{-1}.

High resolution transmission electron microscopy (HRTEM) was performed on a JEM-2010F microscope (JEOL Ltd., Japan), operated at 200 keV. Samples were prepared by ultramicrotomy at room temperature, giving nearly 100 nm thick sections. No further staining was used to improve the contrast. Atomic force microscopy (AFM) was performed on SPA 300HV-DFM (Seiko Instruments Industry Corp., Japan) with a SPI3800 probe station under a tapping mode at room temperature.

The ultraviolet-visible (UV–vis) spectrum of the UV-cured PUA/ZrO_2 film (about 100 μm in thickness) was scanned with a UV–vis spectrophotometer (UV-1800, Shanghai Mei-Pu-Da Instrument Corp., Ltd., China). The refractive index of the UV-cured PUA/ZrO_2 coating was measured by a variable angle ellipsometer (UVISEL, Horiba Jobin Yvon Corp., France) and with a fixed wavelength of 633 nm.

Nanoindentation tests were performed on a Tribo Indenter (Hysitron Corporation, USA) using a three-side pyramid diamond indenter. Loading and unloading rates were set as 10 nm/s and holding time as 5 s. Before each indentation measurement, the tip was calibrated with a standard quartz (reduced elastic modulus 69.6 GPa). Unloading curves were used to analyze the elastic modulus and the hardness of the samples.

Thermogravimetric analyses (TGA) were carried out on Perkin Elmer TGA-7 (USA) at a heating rate of 10 K/min in air.

Results and discussion

Fabrication of PUA/ZrO_2 nanocomposite coatings

In our work, PUA/ZrO_2 nanocomposite coatings were prepared by blending monomers with the prefabricated transparent MPS/ZrO_2 dispersion. Our previous research has already demonstrated that the amount of MPS used is critical for the fabrication of PU/ZrO_2 nanocomposite coatings, which strongly determine the phase separation of ZrO_2 nanoparticles in the coatings and hence the transparency of the nanocomposite coatings [15]. Herein, the

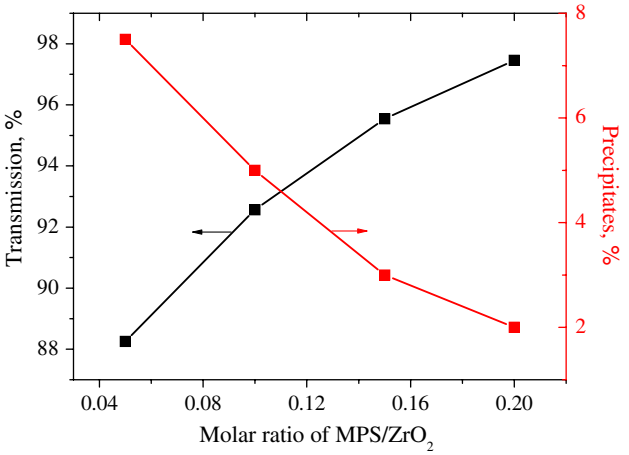

Fig. 1 Effect of molar ratio of MPS/ZrO_2 on the transparency of ZrO_2 dispersion and the precipitates produced at 8000 rpm of centrifugation

effect of the molar ratio of MPS/ZrO_2 on the preparation of ZrO_2/THF dispersions and the transparency of the new PUA/ZrO_2 nanocomposite coatings were also investigated.

Within the range of 0.05:1–0.20:1 of MPS-to-ZrO_2 molar ratio, the effect of MPS-to-ZrO_2 molar ratio on the transparency of ZrO_2/THF dispersions could not be distinguished with naked eyes, but it could be revealed from the transmission at wavelength of 550 nm as illustrated in Fig. 1. Relatively lower transparency of ZrO_2/THF dispersion was acquired at lower molar ratio of MPS/ZrO_2, indicating the existence of ZrO_2 aggregates. To eliminate the influence of ZrO_2 aggregates, all ZrO_2/THF dispersions were centrifuged at 8000 rpm. The amount of precipitates produced by centrifugation is also presented in Fig. 1. Precipitates <8% (based on the total weight of ZrO_2 nanoparticles) were obtained even when the molar ratio of MPS/ZrO_2 was reduced to 0.05:1, suggesting that most of ZrO_2 nanoparticles were successfully de-agglomerated. Moreover, the quantity of the precipitates decreased as the molar ratio of MPS/ZrO_2 increased, confirming that the low transparency of the ZrO_2/THF dispersion is actually caused by the ZrO_2 aggregates.

The ZrO_2/THF dispersions without ZrO_2 aggregates were employed to fabricate PUA/ZrO_2 nanocomposite coatings. Figure 2 gives the transparency of the nanocomposite coatings as a function of ZrO_2 load and molar ratio of MPS/ZrO_2. At low ZrO_2 content, the transparency of the nanocomposite coatings is not influenced by addition of ZrO_2 nanoparticles, in comparison with pure PUA coating. However, it quickly declines with increasing ZrO_2 load when the ZrO_2 load is beyond a certain value, which should be attributed to the phase separation of MPS-functionalized ZrO_2 nanoparticles. It means that a critical ZrO_2 load exists for the fabrication of transparent PUA/ZrO_2 nanocomposite coatings. Figure 2 also shows that the critical ZrO_2 load is about 20 wt% at

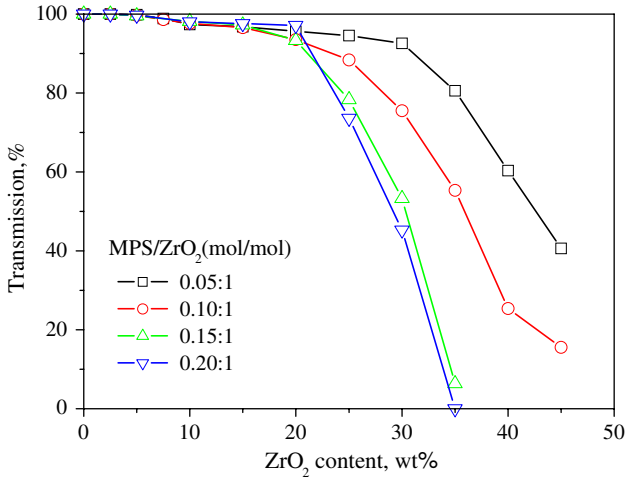

Fig. 2 Effect of molar ratio of MPS/ZrO_2 on the transparency of nanocomposite coatings at wavelength of 550 nm

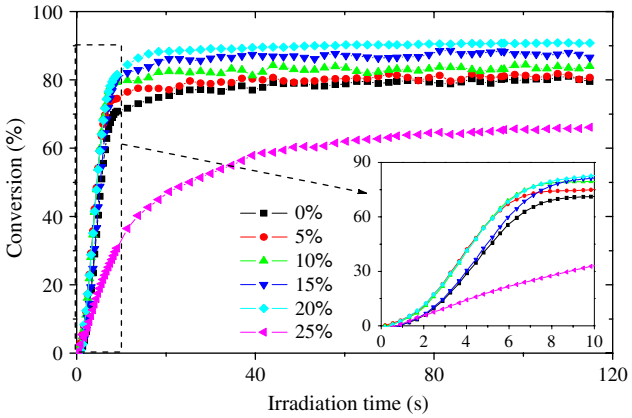

Fig. 3 Photopolymerization profiles of PUA/ZrO_2 nanocomposite coatings with different MPS-ZrO_2 loads (10 mw/cm^2, air, 5 wt% Iragure 184 based on the weight of PUA coating)

MPS-to-ZrO_2 molar ratio of 0.15:1 and 0.20:1 and raises to about 30 wt% at MPS-to-ZrO_2 molar ratio of 0.05:1. Beyond the critical ZrO_2 load, the transparency of the nanocomposite coatings decreases as the molar ratio of MPS/ZrO_2 increases. These facts are the same as those observed in PU/ZrO_2 nanocomposite coatings [15]. That is, the higher the amount of MPS attached to ZrO_2 nanoparticles is, the lower the transparency of the nanocomposite coating is. However, the new PUA/ZrO_2 nanocomposite coating has higher critical ZrO_2 load than PU/ZrO_2 coating, suggesting that addition of active monomers with low molecular weight, such as HDDA, isobornyl acrylate, facilitates for the preparation of transparent nanocomposite coatings with high ZrO_2 load.

Although transparent PUA/ZrO_2 nanocomposite coating with higher ZrO_2 load can be obtained at lower molar ratio of MPS/ZrO_2, a high MPS-to-ZrO_2 molar ratio, 0.20:1, was chosen in the following studies to assure the de-agglomeration of more ZrO_2 nanoparticles and the redispersibility of the MPS-functionalized ZrO_2 nanoparticles. In addition, free MPS molecules were removed to avoid their unexpected influence on the photopolymerization and the properties of nanocomposite coatings.

Effect of MPS-functionalized zirconia nanoparticles on photopolymerization kinetics

The photopolymerization kinetics was monitored by real-time FTIR. The conversion curves as a function of irradiation time for PUA/ZrO_2 nanocomposite coatings as well as pure PUA coating are plotted in Fig. 3. At ZrO_2 content below 20 wt%, the PUA/ZrO_2 nanocomposite coatings, especially with 5, 10, and 20 wt% of ZrO_2 contents, have higher photopolymerization rate than pure PUA coating. Similar phenomenon was also observed in UV-curable polyacrylate/MPS-modified silica nanocomposites at silica content <10 wt% reported by Li et al. [18]. It could be explained by the immobilization of C=C bond on the surface of ZrO_2 nanoparticles. Once these immobilized C=C bonds are initiated in radical polymerization, they are difficult to be deactivated especially via bimacromolecular termination due to their restricted diffusion. As a result of the low termination rate, relatively high photopolymerization rate is acquired finally. The higher curing rate for the coatings with immobilized C=C bonds over with free C=C double bonds has been demonstrated in UV-curable polyacrylate/clay nanocomposites by Owusu-Adom et al. [19]. However, Fig. 3 shows that the polymerization rate of nanocomposite coating considerably decreases and the time to reach polymerization equilibrium is delayed to >50 s (<20 s for other samples) at 25 wt% of ZrO_2 content. Obviously, the opacity of the sample (revealed from its UV–vis spectrum below), and hence the low irradiation intensity attained, are responsible for the low curing rate.

In addition, Fig. 3 indicates that the final conversion steadily increases from 80.5%, 81.7%, 84.1%, 87.5% to 91.3% as ZrO_2 content increases from 0, 5, 10, 15 to 20 wt%, whereas it declines to 68.0% at 25 wt% of ZrO_2. The limited C=C bond conversion is attributed to a vitrification effect during photopolymerization. In our system, the MPS-functionalized ZrO_2 nanoparticles could be regarded as multifunctional monomer. Usually, higher functionality of monomer results in earlier occurrence of vitrification effect and consequently lower final conversion due to the higher cross-linking efficiency. But the coatings studied herein are apparently opposite to this trend. Cho et al. [20] ever reported that limited conversion increased when hydrophilic silica nanoparticles were added into HDDA. They attributed it to the synergistic effect of silica

nanoparticles as an effective flow or diffusion-aid agent during the photopolymerization process and as a contributor toward lengthening the path length of UV light by partial scattering or reflection. Nevertheless, in our opinion, the effective flow or diffusion-aid role of nanoparticles seem to be preposterous because embedding of nanoparticles in coatings generally leads to an increasing viscosity. Additionally, lengthening the path length of UV light is also impossible in our systems since the ZrO_2 nanoparticles have an absolutely small size of $\sim$3.8 nm and, more importantly, they are homogeneously dispersed on primary particle size level (revealing from their TEM images below). With this dispersing state, scattering or reflection of UV light happens with little probability. Therefore, it infers that the increased limited conversion of PUA/ZrO_2 nanocomposite coatings may be caused by the reduced oxygen inhibition because incorporation of ZrO_2 nanoparticles can enhance the barrier property of the coating. The lower final conversion at 25 wt% of ZrO_2 content should be induced by two aspects: the lower polymerization rate and thus the more serious oxygen inhibition, resulting from the shielding effect of ZrO_2 aggregates, and the encapsulation of the immobilized C=C bonds into ZrO_2 aggregates.

Morphology of PUA/ZrO_2 nanocomposite coatings

Within the range of ZrO_2 content investigated, all PUA/ZrO_2 mixtures exhibited transparent and clear appearance when the MPS-functionalized ZrO_2/THF dispersion was just incorporated into PUA mixture. However, after undergoing vacuum-evaporation to remove THF, the sample containing 25 wt% of ZrO_2 transformed into opaque, suggesting the phase separation happened. The dispersion of ZrO_2 nanoparticles in UV-cured film was examined by TEM, as shown in Fig. 4. The images clearly display increasing numbers of ZrO_2 nanoparticles with increasing ZrO_2 content in nanocomposite films. For the samples with 5 and 10 wt% of ZrO_2 (Fig. 4a and b), the nanoparticles are homogeneously dispersed in the films, no significant macroscopic agglomerates are observed. As ZrO_2 content was increased up to 20 wt%, the ZrO_2 agglomerates were inclined to germinate (see the circled region in Fig. 4c). Dense aggregates with size of

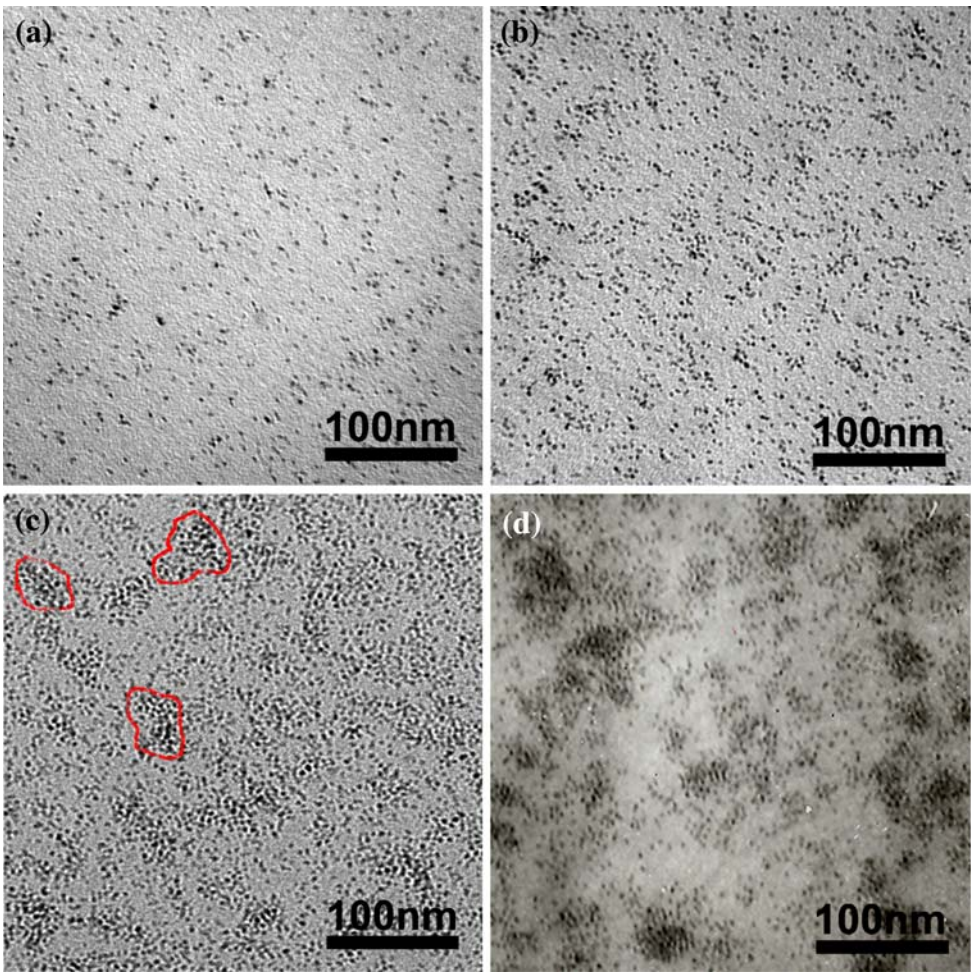

Fig. 4 TEM images of PUA/ZrO_2 nanocomposite films with ZrO_2 content of **a** 5 wt%, **b** 10 wt%, **c** 20 wt%, and **d** 25 wt%

approximate 100 nm were clearly seen in the nanocomposite film with 25 wt% of ZrO_2 (Fig. 4d). So, 20 wt% of ZrO_2 content seems to be the critical concentration for serious phase separation, which is much higher than the value (critical concentration: 10 wt%) for the case only using pure PU oligomer as organic precursor [15]. This result suggests that the existence of isobornyl acrylate and HDDA is favorable for the compatibility of MPS-functionalized ZrO_2 nanoparticles with organic phase.

The surface morphology of PUA/ZrO_2 nanocomposite coatings was probed by AFM technique. Figure 5 typically presents the 2D and 3D images of pure PUA film and PUA/ZrO_2 nanocomposite film with 20 wt% ZrO_2. Both two films show rather smooth surfaces. Quantitative calculation indicates that the surface roughness of PUA film slightly increases from 2.14 to 3.12 nm when 20 wt% of ZrO_2 is incorporated, suggesting the less influence of ZrO_2 nanoparticles on the surface roughness of PUA film. The low surface roughness of nanocomposite film should be attributed to the homogenous dispersion and small size of ZrO_2 nanoparticles, as discussed above.

Optical properties of PUA/ZrO_2 nanocomposite films

The UV–vis transmission spectra of PUA/ZrO_2 nanocomposite films are shown in Fig. 6. In comparison with pure PUA film, the transparency of PU/AZrO_2 nanocomposite films was slightly reduced even at ZrO_2 content up to 20 wt%, but markedly decreased at 25 wt% of ZrO_2, being analogous to the nanocomposite coatings prepared with free MPS-containing ZrO_2/THF dispersion. The high transparency is attributed to the homogeneous dispersion and small size of ZrO_2 nanoparticles while the opacity is resulted from the serious phase separation of ZrO_2 nanoparticles, as revealed from TEM observation. Therefore, similar to the phase separation, 20 wt% is the critical ZrO_2 content for fabrication of transparent nanocomposite film, which is also higher than that (i.e., 10 wt%) we reported before [15]. The high critical ZrO_2 content would be favorable because it means that we can modulate the properties of nanocomposite in a wide range of nanoparticle content without sacrificing the original transparency of polymer film.

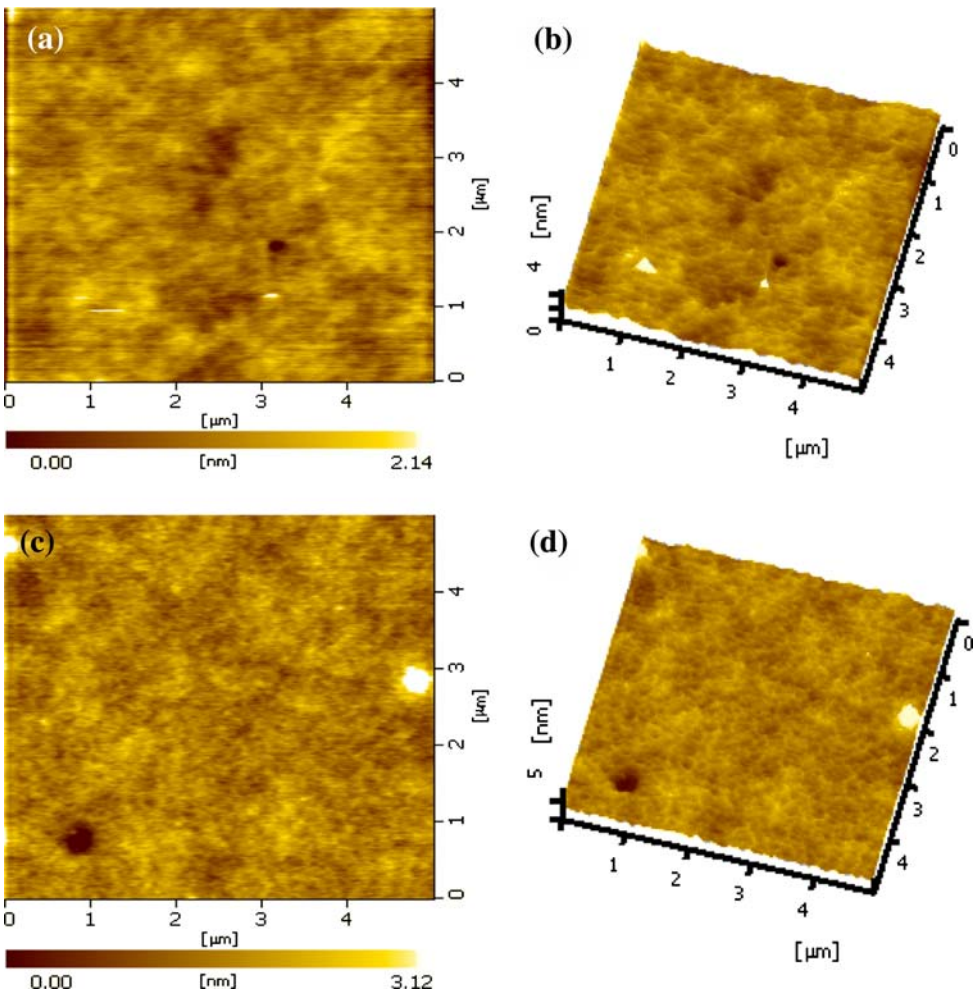

Fig. 5 **a** 2D AFM images of pure PUA film, **b** 3D AFM images of pure PUA film, **c** 2D AFM images of PUA/ZrO_2 nanocomposite film with 20 wt% ZrO_2, and **d** 3D AFM images of PUA/ZrO_2 nanocomposite film with 20 wt% ZrO_2

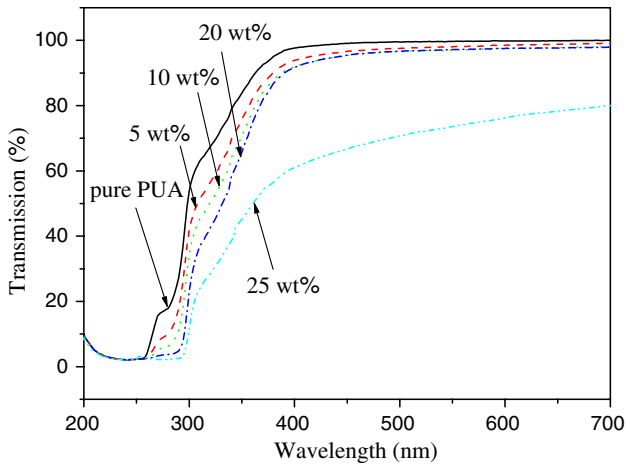

Fig. 6 UV–vis transmission spectra of PUA/ZrO_2 nanocomposite with various ZrO_2 contents

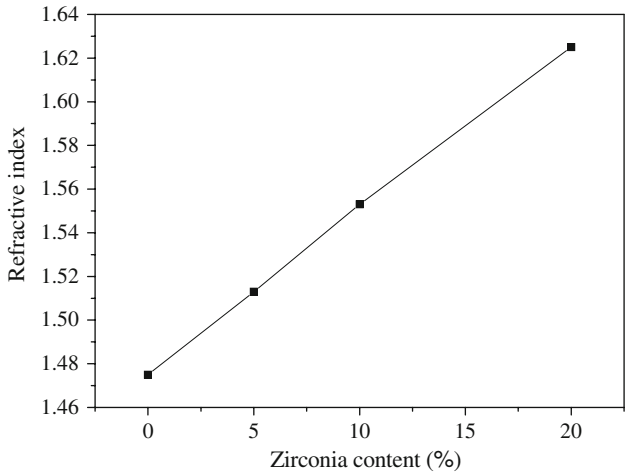

Fig. 7 Refractive indices of PUA/ZrO_2 nanocomposite films with increasing ZrO_2 content

The refractive index of PUA/ZrO_2 nanocomposite films as a function of ZrO_2 content is shown in Fig. 7. It clearly indicates that the refractive index linearly increases with increasing ZrO_2 content, which is differ from the slightly polynomial relationship ever observed for PU/ZrO_2 nanocomposite coatings [15]. The polynomial relationship reported previously may be due to the existence of free MPS molecules which leads to a composition deviation of the organic phase at different ZrO_2 contents. Figure 7 also reveals that a high refractive index of 1.625 is reached at 20 wt% of ZrO_2 content (~6.3 vol.%). Considering the refractive index of 1.475 for pristine PUA film, the efficiency of ZrO_2 nanoparticles for adjusting the refractive index of PUA film is 0.0075 for 1 wt% of ZrO_2 (namely, 0.0238 for 1 vol.% of ZrO_2). This value is approximately twofold of the data reported by Lee et al. [12] wherein an increment of refractive index from 1.39 to 1.65 was obtained after 20.8 vol.% of ZrO_2 was embedded into PDMS, corresponding to 0.0125 for 1 vol.% of ZrO_2. The high efficiency of nonaqueous synthesized ZrO_2 nanoparticles adopted here may be resulted from its highly crystalline and dense structure. The most efficient, however, quite suspectable, enhancement of refractive index via introduction of zirconia component was reported by Sangermano et al. [21] wherein introduction of 5 wt% zirconium tetrapropoxide (namely, 1.88 wt% of ZrO_2) into poly(trimethylolproapane triglycidyl ether) induced an increase of refractive index from 1.477 to 1.580.

Mechanical properties of PUA/ZrO_2 nanocomposite films

Nanoindentation test was employed to study the ZrO_2 load-dependence of the mechanical properties of PUA/ZrO_2 nanocomposites. Figure 8 displays the typical load–displacement curves at a peak indentation load of 5 mN on the PUA/ZrO_2 nanocomposite. A considerable amount of creep strain at the peak load is observed for all samples. Nevertheless, PUA/ZrO_2 nanocomposite film with 20 wt% has the lowest creep strain, consisting with the fact that this sample possesses the highest cross-linking degree revealed from RTIR results. The displacement depth after holding segment is adopted to calculate the hardness (H) and elastic modulus (E) according to the following equations:

$$H = \frac{P_{\max}}{A} \tag{1}$$

$$S = 2\beta\sqrt{\frac{A}{\pi}}E_{\mathrm{r}} \tag{2}$$

where $P_{\max}$ is the maximum load (i.e., 5 mN) and A is the projected contact area; S is the contact stiffness of the material, which is defined as the initial load–displacement slope of the unloading curve; β is a constant depending on the geometry of the indenter, and E_{r} is the reduced elastic modulus based on the following relationship:

$$\frac{1}{E_{\mathrm{r}}} = \frac{1-\nu^2}{E} + \frac{1-\nu_{\mathrm{i}}^2}{E_{\mathrm{i}}} \tag{3}$$

where E_{i} (1140 GPa) and ν_{i} (0.07) are the elastic modulus and Poisson's ratio of the diamond indenter, respectively, and E and ν are the elastic modulus and Poisson's ratio of the sample, respectively.

The results are shown in Fig. 9. It can be seen from the figure that both the hardness and elastic modulus increase with increasing ZrO_2 content up to 20 wt%, demonstrating the reinforcing role of ZrO_2 nanoparticles, especially the sample containing 20 wt% of ZrO_2 has an increase of about 82% on hardness compared with neat PUA. However, the hardness of nanocomposite film yields a considerable

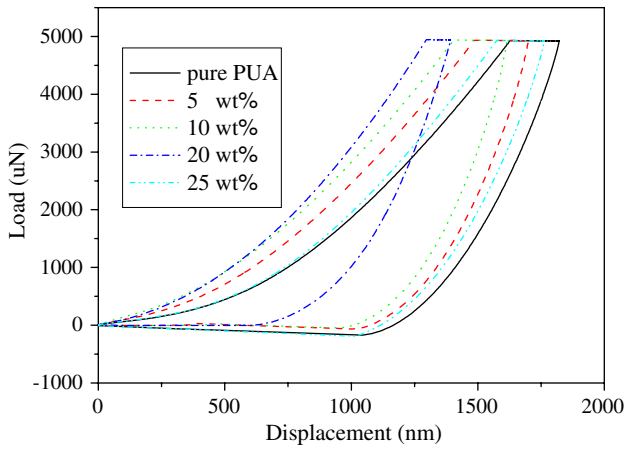

Fig. 8 Load–displacement profiles of pure PUA and PUA/ZrO_2 nanocomposites with increasing ZrO_2 content

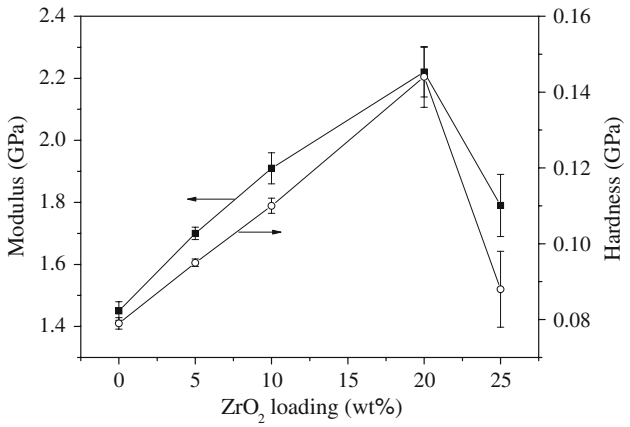

Fig. 9 Effect of ZrO_2 load on the modulus and hardness of PUA film

decrease at 25 wt% of ZrO_2, distinctly indicating the deterioration of the mechanical properties by ZrO_2 agglomeration. For photo-polymerizable formulation, this agglomeration not only decreases the interaction between nanoparticles and polymer matrix, but also leads to a reduction of final C=C bond conversion. Therefore, homogeneous dispersion of nanoparticles is extraordinarily critical to successful fabrication of a UV-curable nanocomposite with high performances.

Thermal properties of PUA/ZrO_2 nanocomposite coatings

Figure 10 illustrates the TGA curves of PUA/ZrO_2 nanocomposite with various ZrO_2 contents. The numbers and range of weight loss stage are quite different for these samples. Pure PUA film has two distinguished weight loss stages: 260–414 °C and 414–536 °C. The former may be due to the cleavages of branch group and urethane bonds and the latter probably due to the decomposition of carbon

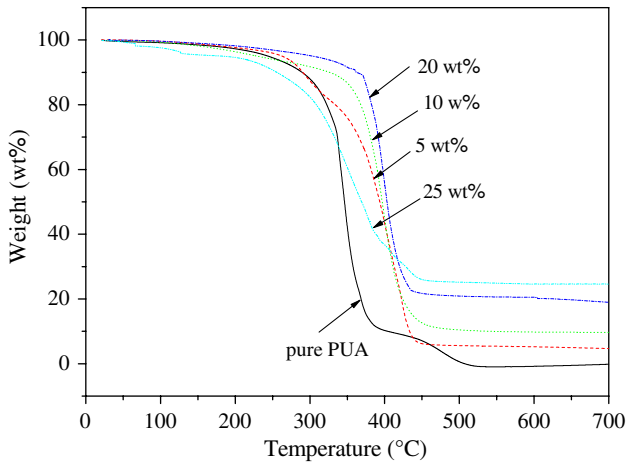

Fig. 10 TGA curves of PUA/ZrO_2 nanocomposite with increasing ZrO_2 content

main chains. The nanocomposite with 5 wt% of ZrO_2 also exhibits a small weight loss stage at 225–325 °C and a main weight loss stage at 325–468 °C. The decomposition at low temperature is close to pure PUA film, which may presumably be attributed to the degradation of the PUA chains residing far from ZrO_2 nanoparticles. Whereas the main weight loss stage is similar to the nanocomposites with 10 and 20 wt%, and thus could be deduced as the degradation of the restrained polymer chains by nanoparticles. The other three samples have one weight loss stage. However, the nanocomposite with 25 wt% of ZrO_2 reached a weight loss of 4.3 wt% especially at low temperature, 130 °C. It should be caused by the evaporation of the entrapped organic solvent in ZrO_2 agglomerates and/or the unreacted monomer because of the low final conversion. The initial decomposition temperature (T_d1 or T_d2), defined as the temperature with 5 wt% of weight loss or the tangential temperature, and the main peak temperature (T_d3) from differential TGA curves for all samples are summarized in Table 1. Except for the sample containing 10 wt%,

Table 1 Summaries of TGA results

ZrO_2 content, wt%	T_d1,[a] °C	T_d2,[a] °C	T_d3,[a] °C	Residue,[b] %
0	244	284	343	0
5	257	270, 367[c]	402	4.68
10	229	367	397	9.66
20	304	361	400	18.9
25	183	277	356	24.5

[a] T_d1, T_d2, and T_d3 are the temperature at 5% of weight loss, the tangential temperature, and the main peak temperature from differential TGA curves, respectively

[b] The remained weight at 700 °C

[c] The initial decomposition temperature of the second weight loss stage

T_d1 increases as the ZrO_2 content increases at ZrO_2 content below 20 wt%. The nanocomposite with 25 wt% of ZrO_2 has a lower T_d1 but a similar T_d2 and T_d3 in comparison with pure PUA film. All other three nanocomposites possess nearly the same T_d2 (the second weight loss stage for the nanocomposite with 5 wt% ZrO_2) and T_d3, both of them are considerably higher than that of pure PUA sample. These data clearly show that MPS-functionalized ZrO_2 nanoparticles can significantly enhance the thermal stability of PUA film. However, their efficient cross-linking with monomers is necessary. Additionally, the T_d2 data disclose that 10 wt% of ZrO_2 nanoparticles is already enough to restrict all organic segments.

The TGA curves also reveal the actual ZrO_2 content in the nanocomposite from the residues. As expected, the residue of the nanocomposite films increases as the amount of ZrO_2 nanoparticles embedded increases. The actual content of ZrO_2 component is a little lower than the quantity of the residues as shown in Table 1, because silica component (about 1.9% of the residues) resulted from the attached MPS segments is included in the residues. Therefore, the real ZrO_2 content in the nanocomposite is apparently less than the theoretical value, this could be attributed to the inherently adsorbed organic component that was counted as ZrO_2 component in the formulation of UV-curable coatings.

Conclusions

A series of completely transparent UV-cured PUA/ZrO_2 nanocomposites were successfully prepared via simple blending with highly dispersible 3-(trimethoxysilyl)propyl methacrylate-functionalized ZrO_2 nanoparticles. Critical ZrO_2 load, depending on the molar ratio of MPS/ZrO_2, was clearly shown for the transparency of the nanocomposite coatings. For the cases using 0.20:1 of MPS-to-ZrO_2 molar ratio, homogeneous dispersion of ZrO_2 nanoparticles in PUA matrix was observed at ZrO_2 content below 20 wt%. As a consequence, the nanocomposites exhibit increases in final C=C double bond conversion, refractive index, hardness, modulus, and thermal stability as ZrO_2 content increases. Particularly, the nanocomposite with 20 wt% of ZrO_2 has extremely high performances, namely, a high refractive index of 1.625, 82% of increment on hardness and about 60 °C higher thermal decomposition temperature relative to pure PUA film. However, at 25 wt% of ZrO_2, ZrO_2 nanoparticles tend to agglomerate in the nanocomposite, leading to serious reduction of the transparency and thus lower final conversion, nearly no improvement on mechanical properties and thermal stability in comparison with pure PUA coating. The homogeneous dispersion of nanoparticles is extremely paramount to get the UV-cured nanocomposite with high performances since it impacts not only the interaction between nanoparticles and polymer matrix, but also the final conversion of the nanocomposite. In addition, this study combining with our previous publication [15] suggests that the highest ZrO_2 concentration for transparent UV-cured nanocomposite can be raised by changing the composition of organic precursors.

Acknowledgements We are grateful for the financial support from the New Century Excellent Talent Foundation of the Ministry of Education of China (NCET-07-0210), National Nature Science Foundation (No. 50703005) of China and Shanghai Leading Academic Discipline Project (No. B113).

References

1. Balazs AC, Emrick T, Russell TP (2006) Science 314:1107. doi:10.1126/science.1130557
2. Sangermano M, Priola A, Kortaberria G, Jimeno A, Garcia I, Mondragon I, Rizza G (2007) Macromol Mater Eng 292:956. doi:10.1002/mame.200700093
3. Okada A, Usuki A (2006) Macromol Mater Eng 291(12):1449. doi:10.1002/mame.200600260
4. Zhou SX, Wu LM, Shen WD, Gu GX (2004) J Mater Sci 39:1593. doi:10.1023/B:JMSC.0000016157.19241.57
5. Zhou SX, Wu LM, Sun J, Shen WD (2002) Prog Org Coat 45:33. doi:10.1016/s0300-9440(02)00085-1
6. Bauer F, Sauerland V, Gläsel HJ, Erns HT, Findeisen M, Hartmann E, Langguth H, Marquardt B, Mehnert R (2002) Macromol Mater Eng 287:546
7. Allen NS, Edge M, Ortega A, Sandoval G, Liauw CM, Verran J, Stratton J, McIntyre RB (2004) Polym Degrad Stabil 85:927. doi:10.1016/j.polymdegradstab.2003.09.024
8. Brickweg LJ, Floryancic BR, Sapper ED, Fernando RH (2007) J Coat Tech 4:107. doi:10.1007/s11998-007-9002-7
9. Xu T, Xie CS (2003) Prog Org Coat 46:297. doi:10.1016/s0300-9440(03)00016-x
10. Yin YJ, Zhou SX, Gu GX, Wu LM (2007) J Mater Sci 42:5959. doi:10.1007/s10853-006-1133-1
11. Zhou HW, Ma J, Li ZC, Chen CH (2005) Chem J Chin Univ 26:1582. doi:cnki:issn:0251-0790.02005-08-049
12. Lee S, Shin HJ, Yoon SM, Yi DK, Choi JY, Paik U (2008) J Mater Chem 18:1751. doi:10.1039/b715338d
13. Garnweitner G, Goldenberg LM, Sakhno OV, Antonietti M, Niederberger M, Stumpe J (2007) Small 3:1626. doi:10.1002/smll.200700075
14. Zhou SX, Garnweitner G, Niederberge M, Antonietti M (2007) Langmuir 23:9178. doi:10.1021/la7000837u
15. Zhou SX, Wu LM (2008) Macromol Chem Phys 209(11):1170. doi:10.1002/macp.200800090
16. Garnweitner G, Niederberger M (2006) J Am Ceram Soc 89:1801. doi:10.1111/j.1551-2916.2006.01005.x
17. Luo KQ, Zhou SX, Wu LM, Gu GX (2008) Langmuir 24(20):11497. doi:10.1021/ia801943n
18. Li FS, Zhou SX, You B, Wu LM (2006) J Appl Polym Sci 99(4):1429. doi:10.1002/app.22629
19. Kwame OA, Guymon CA (2008) Polymer 49(11):2636. doi:10.1016/j.polymer.2008.03.045
20. Cho JD, Ju HT, Hong JW (2005) J Polym Sci Part A Polym Chem 43:658. doi:10.1002/pola.20529
21. Sangermano M, Voit B, Sordo F, Eichhorn KJ, Rizza G (2008) Polymer 49(8):2018. doi:10.1016/j.polymer.2008.03.010